

# UC Riverside

## UC Riverside Previously Published Works

### Title

Endosidin2 targets conserved exocyst complex subunit EXO70 to inhibit exocytosis.

### Permalink

<https://escholarship.org/uc/item/6n05t9w3>

### Journal

Proceedings of the National Academy of Sciences of the United States of America,  
113(1)

### ISSN

0027-8424

### Authors

Zhang, Chunhua  
Brown, Michelle Q  
van de Ven, Wilhelmina  
[et al.](#)

### Publication Date

2016

### DOI

10.1073/pnas.1521248112

Peer reviewed

# Endosidin2 targets conserved exocyst complex subunit EXO70 to inhibit exocytosis

Chunhua Zhang<sup>a,b</sup>, Michelle Q. Brown<sup>a,b</sup>, Wilhelmina van de Ven<sup>a,b</sup>, Zhi-Min Zhang<sup>c</sup>, Bin Wu<sup>d</sup>, Michael C. Young<sup>e</sup>, Lukáš Synek<sup>f</sup>, Dan Borchardt<sup>e</sup>, Reed Harrison<sup>g</sup>, Songqin Pan<sup>a,b</sup>, Nan Luo<sup>a,b</sup>, Yu-ming M. Huang<sup>e</sup>, Yoo-Jin Ghang<sup>e</sup>, Nolan Ung<sup>a,b</sup>, Ruixi Li<sup>a,b</sup>, Jonathan Isley<sup>h,i</sup>, Dimitrios Morikis<sup>g</sup>, Jikui Song<sup>c</sup>, Wei Guo<sup>d</sup>, Richard J. Hooley<sup>e</sup>, Chia-en A. Chang<sup>e</sup>, Zhenbiao Yang<sup>a,b</sup>, Viktor Zarsky<sup>f,j</sup>, Gloria K. Muday<sup>h,i</sup>, Glenn R. Hicks<sup>a,b</sup>, and Natasha V. Raikhel<sup>a,b,1</sup>

<sup>a</sup>Center for Plant Cell Biology, Institute for Integrative Genome Biology, University of California, Riverside, CA 92521; <sup>b</sup>Department of Botany and Plant Sciences, University of California, Riverside, CA 92521; <sup>c</sup>Department of Biochemistry, University of California, Riverside, CA 92521; <sup>d</sup>Department of Biology, University of Pennsylvania, Philadelphia, PA 19104; <sup>e</sup>Department of Chemistry, University of California, Riverside, CA 92521; <sup>f</sup>Institute of Experimental Botany, Academy of Sciences, 165 02 Prague 6, Czech Republic; <sup>g</sup>Department of Bioengineering, University of California, Riverside, CA, 92521; <sup>h</sup>Department of Biology, Wake Forest University, Winston-Salem, NC 27109; <sup>i</sup>Center for Molecular Communication and Signaling, Wake Forest University, Winston-Salem, NC 27109; and <sup>j</sup>Department of Experimental Plant Biology, Faculty of Sciences, Charles University, 128 43 Prague 2, Czech Republic

Contributed by Natasha V. Raikhel, October 29, 2015 (sent for review September 28, 2015)

**The exocyst complex regulates the last steps of exocytosis, which is essential to organisms across kingdoms. In humans, its dysfunction is correlated with several significant diseases, such as diabetes and cancer progression. Investigation of the dynamic regulation of the evolutionarily conserved exocyst-related processes using mutants in genetically tractable organisms such as *Arabidopsis thaliana* is limited by the lethality or the severity of phenotypes. We discovered that the small molecule Endosidin2 (ES2) binds to the EXO70 (exocyst component of 70 kDa) subunit of the exocyst complex, resulting in inhibition of exocytosis and endosomal recycling in both plant and human cells and enhancement of plant vacuolar trafficking. An EXO70 protein with a C-terminal truncation results in dominant ES2 resistance, uncovering possible distinct regulatory roles for the N terminus of the protein. This study not only provides a valuable tool in studying exocytosis regulation but also offers a potentially new target for drugs aimed at addressing human disease.**

endosidin2 | exocytosis | exocyst | EXO70

**T**he EXO70 (exocyst component of 70 kDa) protein is a component of the evolutionarily conserved octameric exocyst complex that tethers post-Golgi vesicles to the plasma membrane before SNARE-mediated membrane fusion (1). As an important component of the exocyst complex that mediates exocytosis, EXO70 regulates, for example, neurite outgrowth, epithelial cell polarity establishment, cell motility, and cell morphogenesis in animal cells (2–6). In plants, EXO70 proteins participate in polarized pollen tube growth, root hair growth, deposition of cell wall material, cell plate initiation and maturation, defense, and autophagy (7–12). In humans, EXO70 mediates the trafficking of the glucose transporter Glut4 to the plasma membrane that is stimulated by insulin and involved in the development of diabetes (13). A specific isoform of human EXO70 is also involved in cancer cell invasion (13–15). Endosidin2 (ES2) was identified from a plant-based chemical screen as an inhibitor of trafficking. We demonstrate that the target of ES2 is the EXO70 subunit of the exocyst and that ES2 is active in plants and mammalian systems. Significantly, no inhibitor of the exocyst complex has been reported, yet such compounds could be important for understanding the basic mechanisms of exocyst-mediated processes, for modifying secretion in biotechnological applications, and for the development of potential new drugs with higher affinity and more potent activity to control exocyst-related diseases.

## Results

**ES2 Inhibits Trafficking to the Plasma Membrane.** ES2 is a previously identified plant endomembrane trafficking disruptor (Fig. 1A) that inhibits polarized growth of pollen tubes in a dose-dependent manner (Fig. S1 A and B) (16). *Arabidopsis* seedlings grown on media containing ES2 have shorter roots and fewer and shorter

root hairs and are less sensitive to gravity stimulation (Fig. S1 C–G). ES2 disrupted the trafficking of proteins that are actively recycled between the plasma membrane and endosomes, such as the brassinosteroid receptor (BRI1) and the auxin transporters PINFORMED1 (PIN1) and PIN2 after short time treatment (2 h) (Fig. S2A) (16, 17). Although ES2 was originally identified from the same phenotype cluster as bioactive compounds ES1 and ES3, it did not target the same proteins as ES1 and ES3 because it did not induce aggregation of trans-Golgi network marker SYP61 compared with ES1 and did not affect ROP6 localization compared with ES3, respectively (Fig. S2A) (16, 17). ES2 also did not affect the localization of cellular markers such as HDEL:GFP [endoplasmic reticulum (ER)], GOT1p:YFP (Golgi), SYP22:YFP [tonoplast and prevacuolar compartment (PVC)], PGP4:GFP (plasma membrane), or PIP2a:GFP (plasma membrane) (Fig. S2B).

We further explored ES2 effects at the cellular level using GFP-tagged PIN2 protein because it is known to traffic to the plasma membrane, endosomes, and vacuoles (18–21). Short term ES2 treatment reduced the amount of the plasma membrane-localized PIN2 compared with control seedlings, as shown by a fluorescence intensity plot profile in time-lapse images of PIN2:GFP seedlings

## Significance

**The exocyst complex is a conserved protein complex that tethers the secretory vesicles to the site of membrane fusion during exocytosis, an essential cellular process that transports molecules, such as protein, to the cell surface or extracellular space. We identified a small molecule that targets the EXO70 (exocyst component of 70 kDa) subunit of the exocyst complex to inhibit exocytosis. This compound made it possible to control the dynamics of the exocytosis process in a dosage-dependent manner in different organisms and overcame the mutant lethality and genetic redundancy issues in studying mechanisms of exocyst complex regulation. Further design of molecules with higher affinity and more potent activity may make it possible to use drugs to control human diseases related to exocytosis, such as cancer and diabetes.**

Author contributions: C.Z., M.Q.B., W.v.d.V., M.C.Y., D.M., J.S., W.G., R.J.H., C.A.C., Z.Y., V.Z., G.K.M., G.R.H., and N.V.R. designed research; C.Z., M.Q.B., W.v.d.V., Z.-M.Z., B.W., M.C.Y., L.S., D.B., R.H., S.P., N.L., Y.-m.M.H., Y.-J.G., N.U., R.L., and J.I. performed research; C.Z., D.B., and R.H. analyzed data; and C.Z. and G.R.H. wrote the paper.

The authors declare no conflict of interest.

Freely available online through the PNAS open access option.

Data deposition: The atomic coordinates and structure factors have been deposited in the Protein Data Bank, [www.pdb.org](http://www.pdb.org) [PDB ID code 4RL5].

See Commentary on page 14.

<sup>1</sup>To whom correspondence should be addressed. Email: [natasha.raikhel@ucr.edu](mailto:natasha.raikhel@ucr.edu).

This article contains supporting information online at [www.pnas.org/lookup/suppl/doi:10.1073/pnas.1521248112/-DCSupplemental](http://www.pnas.org/lookup/suppl/doi:10.1073/pnas.1521248112/-DCSupplemental).

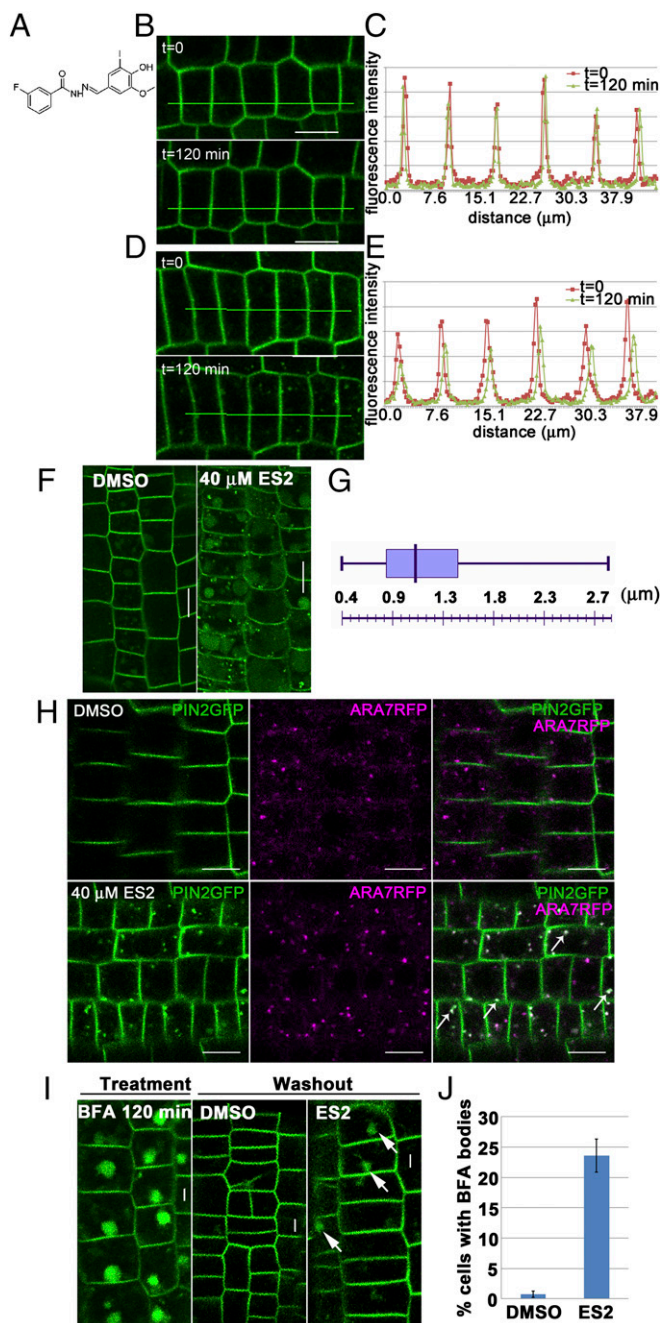


**Fig. 1.** ES2 inhibits trafficking to the plasma membrane, and trafficking to the vacuole is increased as a consequence in *Arabidopsis*. (A) ES2 molecular structure. (B) Time course images of PIN2 localization in root epidermal cells treated with 0.5% DMSO at time 0 (Top) and time 120 min (Bottom) under normal light conditions. The lines in the cross-section of the images show the location of plot profile shown in C. (C) Plot profile of the lines shown in images in B. The fluorescence intensity along the line at time 0 is shown in red, and that along the line at time 120 min is shown in green. B and C show that the fluorescence intensity of PIN2 at the plasma membrane is not significantly altered over a time course of 2 h. (D) Time course images of PIN2 localization in root epidermal cells treated with 40  $\mu$ M ES2 at time 0 (Top) and time 120 min (Bottom) under normal light conditions. The lines in the cross-section of the images show the location of the plot profile shown in E. (E) Plot profile of the lines shown in images in D. The fluorescence intensity along the line at time 0 is shown in red, and that along the line at time 120 min is shown in green. D and E show that the fluorescence intensity of PIN2 at the plasma membrane is reduced after 2 h of ES2 treatment. (F) PIN2 trafficking to the vacuole is increased after ES2 treatment. Images show root cells from PIN2::PIN2:GFP seedlings treated with 0.5% DMSO (Left) or 40  $\mu$ M

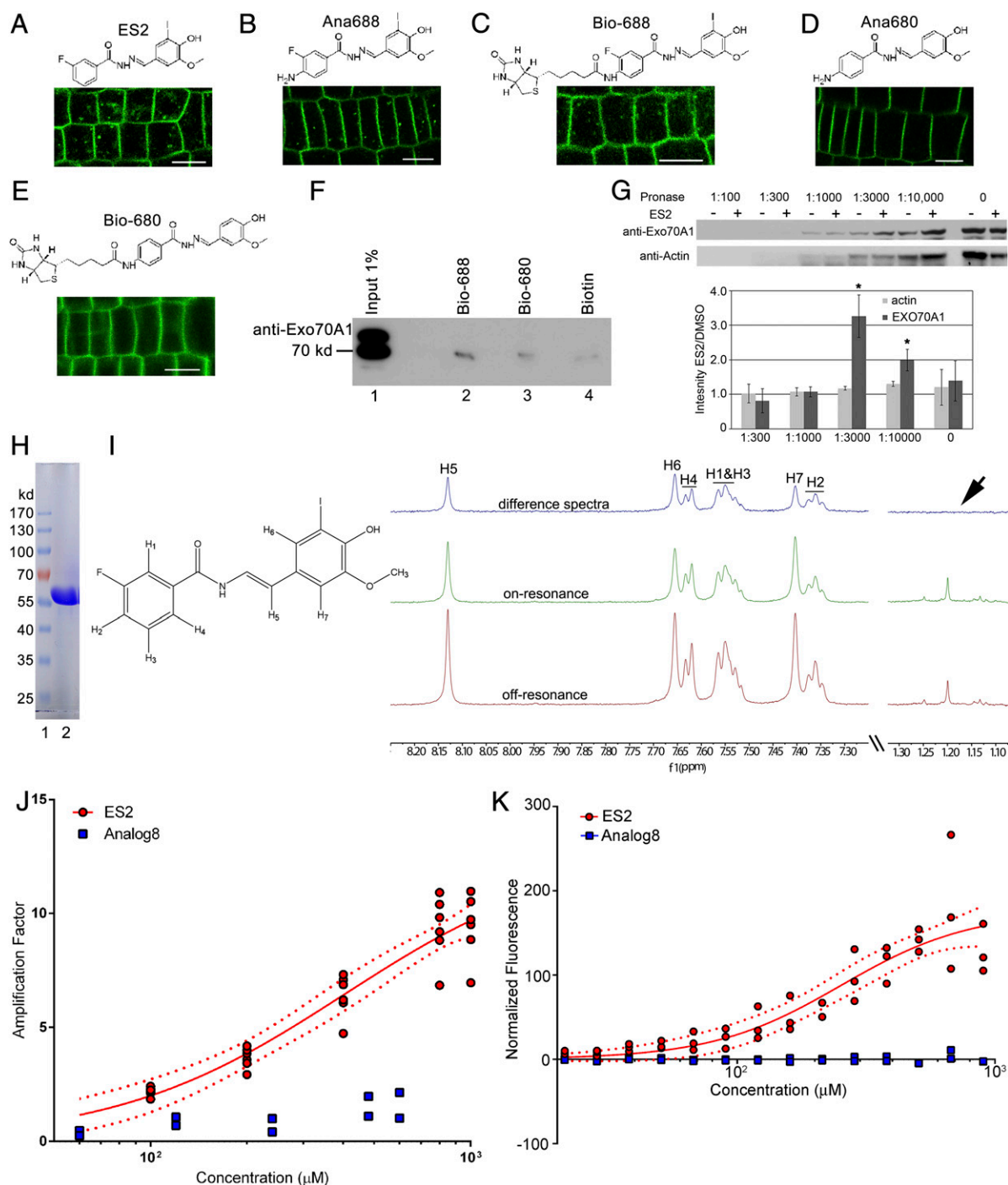
treated with DMSO or ES2 (Fig. 1 B–E). The mean fluorescence intensity of total plasma membrane-localized PIN2:GFP in seedlings treated with ES2 ( $90.6 \pm 13.7$ , mean  $\pm$  SD,  $n = 30$ ) was significantly lower than that in seedlings treated with DMSO ( $118.3 \pm 17.9$ , mean  $\pm$  SD,  $n = 30$ ) ( $P < 0.05$ ). When we performed ES2 treatment of PIN2::PIN2:GFP-expressing seedlings in the dark to inhibit vacuolar-localized GFP fusion protein degradation (22), we found an increased amount of GFP fluorescence in the vacuoles compared with the control (Fig. 1F). The results indicated that ES2 treatment inhibited trafficking to the plasma membrane, and, as a consequence, the trafficking to the vacuole for degradation is enhanced.

The feret diameter of PIN2-localized compartments observed from fluorescence confocal microscope images upon ES2 treatment under light conditions was  $1.18 \pm 0.47 \mu$ m (mean  $\pm$  SD,  $n = 391$ , from 107 cells of 11 seedlings), with a maximum feret diameter of 2.9  $\mu$ m and a minimal feret diameter of 0.4  $\mu$ m (Fig. 1G). Size distribution of ES2-induced PIN2 agglomerations indicates that they are very different from known brefeldin A (BFA)-induced agglomerations resulting from abnormal trafficking at the Golgi. PIN2 vacuolar trafficking involves the retromer complex, including its component Sorting Nexin1 that colocalizes with ARA7/RabF2b endosomes (19, 20). We found that, in seedlings expressing both PIN2::PIN2:GFP and ARA7/RabF2b:mRFP, the ES2 treatment induced PIN2 accumulation in the ARA7/RabF2b endosomal compartments (Fig. 1H). We manually examined 338 PIN2 agglomerations from roots of 12 seedlings treated with ES2 and found that all of these agglomerations had partial or complete colocalization with ARA7/RabF2b-labeled late endosomes/PVC. Accumulation of PIN2 in ARA7/RabF2b-positive compartments was consistent with our observation that ES2 reduced PIN2 plasma membrane localization and that PIN2 trafficking to the vacuole is increased.

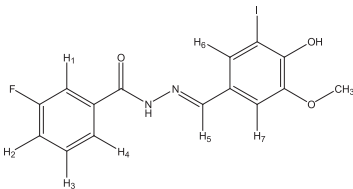
We next examined whether a reduced quantity of PIN2 at the plasma membrane was a result of reduced PIN2 recycling. The PIN2::PIN2:GFP seedlings grown on normal media were treated with BFA for 2 h and then permitted to recover in liquid media containing either ES2 or DMSO for another 1.5 h before imaging. We found that the disappearance of BFA bodies in ES2-treated seedlings showed a significant delay in comparison with the DMSO containing media (Fig. 1I and J), indicating that ES2 treatment reduced PIN2 recycling through endosomes. Similar delayed PIN2 recycling has been observed in mutants that are defective in exocytosis (23).

The ES2 molecule contains an *N*-acyl hydrazone group at its core and could have the propensity for hydrolysis to 3-fluorobenzohydrazide and 4-hydroxy-3-iodo-5-methoxybenzaldehyde in aqueous solution (Fig. S3A). To confirm whether ES2 is stable in our system, we tested the stability of ES2 in a water solution using  $^1$ H NMR analysis. We collected  $^1$ H NMR spectra of ES2 at different time points over a course of 1 wk and observed no hydrolysis products under these conditions (Fig. S3B). In addition, we tested the activity of the two possible ES2 hydrolysis products in inducing PIN2 localization in late endosomal compartments. We

ES2 (Right) for 2 h in the dark. (G) Box plot showing the size distribution of PIN2 agglomerations after ES2 treatment. (H) ES2-induced PIN2 agglomerations colocalize with ARA7/RabF2b. (Top) Images from PIN2::PIN2:GFP;ARA7/RabF2b:mRFP root cells treated with 0.5% DMSO, showing GFP channel, mRFP channel, and merged channel from Left to Right. (Bottom) Images from PIN2::PIN2:GFP;ARA7/RabF2b:mRFP root cells treated with 40  $\mu$ M ES2, showing GFP channel, mRFP channel, and merged channel from Left to Right. (I) ES2 reduces recycling efficiency of BFA-induced PIN2-positive membrane aggregates. (Left) PIN2 localization after BFA treatment. (Middle) PIN2 localization after 90 min of recovery in normal 0.5 $\times$  MS media. (Right) PIN2 localization after 90 min of recovery in 0.5 $\times$  MS media containing 40  $\mu$ M ES2. Arrows show the residual PIN2 aggregates. (J) Quantification of cells containing BFA compartments after recovery in media containing DMSO or ES2. (Scale bars: 10  $\mu$ m.)



**Fig. 2.** ES2 interacts with the EXO70A1 subunit of the exocyst complex. (*A–E*) Structure and bioactivity of ES2 and its synthesized analogs. *Top* are the structures and *Bottom* are the PIN2 localization after treatment with 40  $\mu\text{M}$  of corresponding analogs. Bio-688 (*C*, active) and Bio-680 (*E*, inactive) were used in pull-down assays. (Scale bars: 10  $\mu\text{m}$ .) (*F*) Western blot detection of EXO70A1 in the resin from the pull-down assays using anti-EXO70A1 antibody. Lane 1, 1% of the input sample; lane 2, resin from the Bio-688 sample; lane 3, resin from the Bio-680 sample; lane 4, resin from the free Biotin sample. (*G*) DARTS assay shows that ES2 protects EXO70A1, but not actin, from degradation. (*Top*) Western blot of DARTS samples treated with different concentrations of pronase using anti-EXO70A1 and anti-actin antibodies. The chart at the *Bottom* shows the signal intensity ratio between ES2 and DMSO using antibodies against EXO70A1 and actin under different dilutions of pronase. At 10,000 and 3,000 dilutions, EXO70A1 protein was obviously protected from degradation by ES2. The error bars represent SEs of two independent experiments. (*H*) Coomassie staining of purified EXO70A1 protein (amino acid 75 to end) used for STD-NMR experiments. (*I*) ES2  $^1\text{H}$  assignment and the spectra of STD-NMR using purified EXO70A1 protein and ES2. Red, green, and blue colors represent off resonance, on resonance, and different spectrum, respectively. The arrow indicates a spectral peak from the buffer component present in the sample. The signal from the buffer is not present in the different spectrum. (*J*) STD-NMR binding curves of EXO70A1 titrated with different concentrations of ES2 (red) and analog8 (blue). Red circles represent STD amplification factors of ES2 H1 through H7 dosed with ES2. Blue squares represent STD amplification factors of analog8 H2a, H2b, and CH3 dosed with analog8. Solid lines represent the nonlinear fit curves, and the dotted lines represent the 95% confidence interval of the fit. (*K*) Thermophoresis binding curves of NT-647-labeled EXO70A1 titrated with different concentrations of ES2 (red) and analog8 (blue). Red circles and blue squares represent normalized fluorescence of EXO70A1 dosed with ES2 and analog8, respectively, from each replicate experiment. Solid lines represent the nonlinear fit curves, and the dotted lines around the fit represent the 95% confidence interval of the fit.

**Table 1. ES2 <sup>1</sup>H NMR chemical shifts**


Number	ES2 <sup>1</sup> H chemical shifts, d(ppm)	
	DMSO- <i>d</i> <sub>6</sub>	D <sub>2</sub> O
1	7.70	7.49
2	7.45	7.29
3	7.59	7.46
4	7.76	7.55
5	8.29	8.06
6	7.61	7.59
7	7.33	7.33
NH	10.09	NA
CH3	3.89	3.79
OH	NA	NA

NA, not available; ppm, parts per million.

found PIN2 localization at the plasma membrane after we treated PIN2::PIN2:GFP seedlings with 40 μM 3-fluorobenzohydrazide or 4-hydroxy-3-iodo-5-methoxybenzaldehyde for 2 h, similar to what we observed in the DMSO control, but significantly different from the intracellular localization pattern in ES2 treated samples (Fig. S3 C–F). These data showed that ES2 is a stable compound under aqueous solution and that the induced trafficking phenotypes are not due to any in situ hydrolysis byproducts.

Overall, we concluded that ES2 reduced trafficking to the plasma membrane and that protein trafficking to the vacuole is increased as a consequence. This observation suggests a possible mechanism to regulate the dynamics of vesicle trafficking.

**EXO70A1 is a Cellular Target of ES2.** Structure-activity relationship (SAR) analysis was performed to identify moieties in ES2 that were dispensable for its activity based on the induction of PIN2 localization in agglomerations (Fig. 2A and Fig. S4). We found that the iodine in the molecule was necessary for its activity whereas the benzoic ring with the fluorine could accommodate different atoms while maintaining activity. To generate analogs with biotin to facilitate target identification, we synthesized new active and inactive analogs with an amine group in the benzoic ring with the fluorine named analog-688 (Ana-688) and analog-680 (Ana-680), as active and inactive analogs, respectively (Fig. 2B and D). These two analogs were further modified to produce biotinylated molecules using the amine group and named Bio-688 and Bio-680, respectively (Fig. 2C and E) (see *SI Materials and Methods* for schemes and *Dataset S1* for characterization of synthesized compounds). Ana-688 and Bio-688 induced PIN2 agglomerations after short-term treatment whereas Ana-680 and Bio-680 did not, indicating they could be used as active analogs and inactive analogs, respectively.

Bio-688 and Bio-680 were coupled to streptavidin agarose, resulting in active and inactive matrices, respectively, which were incubated with *Arabidopsis* cell extracts. Proteins bound to the active and inactive matrices were eluted by ES2, and the eluted fractions were analyzed using mass spectrometry (MS). Although the peptide abundance in the elution fractions was low (*Dataset S2*), we detected a peptide from *Arabidopsis* EXO70G2, which belongs to the EXO70 family in *Arabidopsis* that is involved in exocytosis, from the active matrix but not the inactive matrix elution. EXO70G2 belongs to the EXO70 family that has 23 members in *Arabidopsis* divided into subclasses A to H (7, 24,

25). EXO70A1, which shares 24% amino acid sequence identity with that of EXO70G2, is a member of the EXO70 family that has been well-studied, and there are resources available for us to do further investigation. We then took other approaches to test for possible interaction between ES2 and EXO70 proteins in *Arabidopsis*. Using an available EXO70 antibody, we further tested the presence of a close paralog EXO70A1 on the matrix by Western blot (Fig. 2F) (7–9, 23, 26). The intensity of the Western blot bands indicated that the Bio-688 matrix was more potent in pulling down EXO70A1, in comparison with the Bio-680 matrix and biotin controls, indicating that EXO70A1 interacted more strongly with the active ES2 analog compared with the inactive analog.

We took a relatively new approach for chemical target identification called drug affinity responsive target stability (DARTS) to test the interaction between ES2 and EXO70A1 (27). The DARTS approach was developed based on the observation that some proteins are protected from degradation by proteases when bound to the ligand (27). We incubated an *Arabidopsis* protein extract with ES2 or DMSO and then digested with different concentrations of proteases. After normalizing EXO70A1 protein Western blot band intensity against that of the actin internal control, we found that the degradation of EXO70A1 was significantly protected by ES2 compared with actin, which was detected on the same blotting membrane at protease dilutions of 1:3,000 and 1:10,000 (Fig. 2G). We further expressed and purified the EXO70A1 protein from *Escherichia coli* and tested for its interaction with ES2, using saturation-transfer difference NMR (STD-NMR) (28). EXO70A1 amino acid residues 75–638 were used for STD-NMR due to the instability of the full-length protein (Fig. 2H). The <sup>1</sup>H assignments of ES2 in DMSO-*d*<sub>6</sub> were determined from gCOSY (gradient correlation spectroscopy) and gNOESY (gradient nuclear overhauser effect spectroscopy) spectral analysis (Fig. S5 A and B and Table 1). Assignments in D<sub>2</sub>O were made by comparison with the 1D spectrum recorded in DMSO-*d*<sub>6</sub>. To determine the optimum saturation time, an STD build-up curve was generated using 400 μM ES2 and 20 μM EXO70A1 samples (Fig. S6C). The build-up curve (Fig. 2I) clearly indicated that there was direct interaction between ES2 and EXO70A1. The <sup>1</sup>H spectral peak from an unrelated molecule showed no interaction with EXO70A1 (Fig. 2I, arrow). Based on the results from the build-up curve, all further STD-NMR measurements were taken using a 2-s saturation time. We titrated EXO70A1 with different concentrations of ES2 in an STD-NMR experiment, and the STD amplification factor was calculated as a function of ES2 concentration (Fig. 2J). The dissociation constant (*K*<sub>d</sub>) of the EXO70A1 and ES2 interaction using STD-NMR was 400 ± 170 μM and the *B*<sub>max</sub> was 12.9 ± 2.74 (Table 2). We also performed the <sup>1</sup>H assignments of ES2 analog8 (Table S1 and Fig. S5D), an inactive analog, and studied the interaction between analog8 and EXO70A1 using STD-NMR. The calculated STD amplification factors did not show a significant increase, with elevated concentrations of analog8 (Fig. 2J). This result confirmed that the detected interaction between ES2 and EXO70A1 using STD-NMR is not due to random interaction of any small molecule with EXO70A1 protein.

**Table 2. Nonlinear fit summary of ES2 binding curves using STD-NMR and MST**

Parameters	STD EXO70A1	MST	
		EXO70A1	EXO70A1-L596A;I613A
<i>B</i> <sub>max</sub> , μM (mean ± SE)	12.9 ± 2.74	176 ± 26.9	96.9 ± 16.9
<i>h</i>	1.21 ± 0.297	1.73 ± 0.436	4.13 ± 2.85
<i>K</i> <sub>d</sub> , μM (mean ± SE)	400 ± 170	253 ± 63.6	252 ± 50.6
R square, %	90.2	81.7	46.5

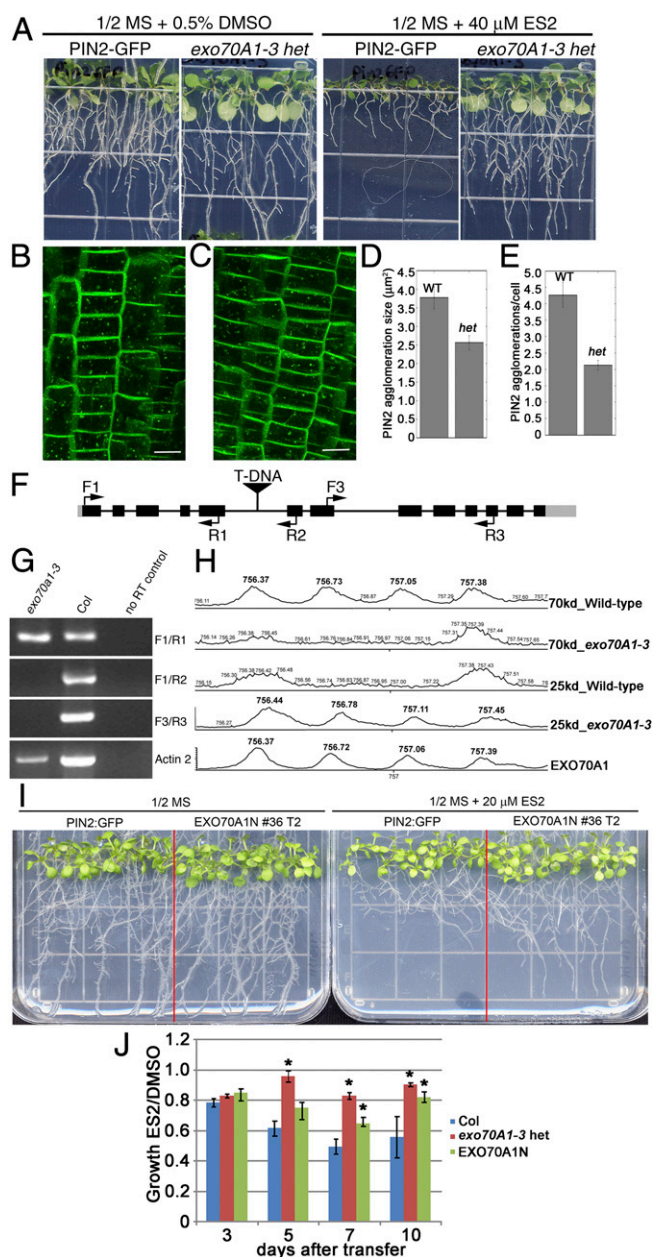


**Fig. 3.** EXO70A1 N-terminal peptide contributes to ES2 resistance. (A) Heterozygous mutant allele of *exo70A1-3* displays resistance to ES2. (B) WT seedlings from EXO70A1 heterozygous progeny expressing PIN2::PIN2:GFP treated with 40  $\mu$ M ES2 for 2 h. (C) Heterozygous seedlings from EXO70A1 heterozygous progeny expressing PIN2::PIN2:GFP treated with 40  $\mu$ M ES2 for 2 h. (D) Heterozygous mutant allele of *exo70A1-3* ( $n = 370$  cells from 16 seedlings) has smaller PIN2 agglomerations compared with WT seedlings ( $n = 241$  cells from 12 seedlings) in the same segregating population ( $P < 0.001$ ). (E) Heterozygous mutant allele of *exo70A1-3* ( $n = 370$  cells from 16 seedlings) has fewer numbers of PIN2 agglomerations compared with WT seedlings ( $n = 241$  cells from 12 seedlings) in the same population ( $P < 0.001$ ). (F) Diagram showing the EXO70A1 gene organization and the location of the T-DNA insertion in the *exo70A1-3* allele. The arrows mark locations and orientations of the primers used for allele characterization in G. (G) RT-PCR shows that T-DNA insertion causes accumulation of truncated EXO70A1 mRNA in homozygous *exo70A1-3* seedlings. EXO70A1 mRNA sequence 3' of the T-DNA insertion site was not detected. (H) MS spectra of extracted ion chromatograms of  $m/z$  756.43,3+ for the peptide spanning amino acids 90–109 of EXO70A1 from protein gel bands of WT or *exo70A1-3*. The EXO70A1 N-terminal peptide (amino acids 90–109) was detected in the 70-kDa region but not the 25-kDa region from WT plants; the same peptide was detected in the 25-kDa region but not the 70-kDa region from *exo70A1-3* homozygous

To further confirm results from STD-NMR, we used the technique of microscale thermophoresis (MST) to quantify the dissociation constant for the complex of ES2 (titrant) with EXO70A1 (target molecule). This method observes the motion of molecules in response to a temperature gradient (29–31). Thermophoresis is characterized by monitoring the time-dependent fluorescence, referred to as a time trace, of a labeled target molecule in a small zone subject to localized heating by an infrared laser (30). Multiple time traces were acquired for serial dilutions of a binding partner. Because binding of the titrant with the target molecule results in a change of mass, charge, or hydration entropy, the complex exhibits different thermophoretic behavior from the target molecule alone (29, 31). Plotting the thermophoretic effect as a function of titrant concentration presents dose-dependent behavior. From the dose-responsive curve, we calculated a  $K_d$  of  $253 \pm 63.5 \mu\text{M}$  for the interaction of ES2 with EXO70A1. Although the mean value from MST is lower than the  $K_d$  from STD-NMR, the results are not significantly different with a 95% level of confidence. This result suggests a micromolar affinity for the binding of ES2 to EXO70A1 consistent between binding assays based on different physical principles (Table 2). Moreover, when MST is performed for the interaction of a negative control, analog8, with EXO70A1, we observed no change in thermophoretic behavior as expected (Fig. 2K).

We concluded from these different assays that ES2 interacted with EXO70A1 in vitro, suggesting that it could be a target in vivo.

**The Expression of EXO70A1 N Terminus Results in Desensitization to ES2.** To investigate the relationship between ES2 and the EXO70 gene family at the genetic level, we tested root growth phenotypes of available *exo70* mutants as listed in Table S2, in the presence of ES2. None of the 24 mutants that we tested displayed significant differences in response to ES2 compared with WT, except one. Heterozygous seedlings of T-DNA (transfer DNA) insertion allele *exo70A1-3* (SALK\_026036C) showed resistance to ES2 in root growth (Fig. 3A). To study the response of T-DNA insertion mutant plants to ES2 at the cellular level, we crossed PIN2::PIN2:GFP with *exo70A1-3* heterozygous plants. The F3 population from an F2 seedling that was homozygous for PIN2::PIN2:GFP and heterozygous for T-DNA insertion was used to study the difference between WT plants and *exo70A1-3* heterozygous plants. Upon ES2 treatment, heterozygous T-DNA insertion mutant seedlings showed smaller and fewer PIN2 agglomerations compared with WT seedlings from the same segregating population (Fig. 3B–E). Although heterozygous *exo70A1-3* seedlings had normal growth at the seedling stage, the plants had retarded growth after bolting, more shoot stems, reduced seed yield, and abnormal flower development (Fig. S6A). Homozygous *exo70A1-3* seedlings had severe growth phenotypes that included arrested root growth and abnormal root meristem organization and were seedling lethal (Fig. S6B), similar to previously characterized *exo70A1-1* and *exo70A1-2* mutant alleles, but were more severe (7). The more severe phenotypes in *exo70A1-3* homozygous plants were reported previously, and it was not understood why this T-DNA insertion

plants. (I) Transgenic plants that express EXO70A1 N-terminal peptide (amino acids 1–231) are less sensitive to ES2 in root elongation. The transgenic plants have longer roots in comparison with the PIN2::PIN2:GFP line on 20  $\mu$ M ES2 plates. (J) The ratio of root growth on 30  $\mu$ M ES2 relative to 0.5% DMSO in different genotypes was calculated at different time points after being transferred. Col, *exo70A1-3* heterozygous and EXO70A1N seeds were grown on 1/2 MS agar plates for 3 d, and the seedlings were then transferred to 1/2 MS agar plates containing 0.5% DMSO or 30  $\mu$ M ES2. The absolute root growth of each seedling after transfer was calculated at different time points. The ratio of root growth on 30  $\mu$ M ES2 relative to the root growth on DMSO was calculated for each genotype at each time point. The \* represents a significant difference to Col in  $t$  test ( $P < 0.05$ ). (Scale bars: B and C, 10  $\mu$ m.)

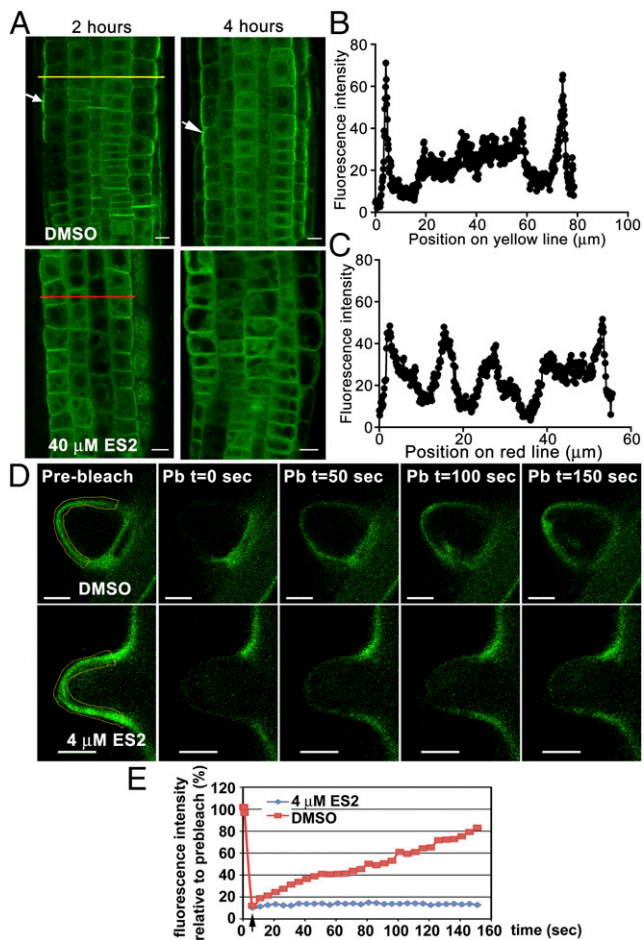


**Fig. 4.** ES2 inhibits EXO70A1 dynamics in *Arabidopsis* root cells. (A) EXO70A1 has a polar localization pattern on the outer lateral side of the root epidermal cells in the transition zone, and this pattern is altered by ES2 treatment. Localization of EXO70A1 in the transition zone after 2 h or 4 h of treatment with DMSO (Top) or ES2 (Bottom) was shown. (B) Plot profiles of fluorescence intensity across the yellow lines in DMSO-treated sample as shown in A. (C) Plot profile of fluorescence intensity across the red line in ES2-treated sample as shown in A. (D) Images of fluorescence recovery after photobleaching (FRAP) analysis in root hair cells treated with 0.05% DMSO (Top) or 4  $\mu$ M ES2 (Bottom). Pre-bleach represents the fluorescence before photo bleaching. Pb represents the time point of post-bleach recovery. The yellow shapes in Prebleach images indicate the regions that were manually selected for photo bleaching. (E) Plot of relative fluorescence intensity to prebleaching at different time points in ES2-treated and control cells shown in D. (Scale bars: 10  $\mu$ m.)

line caused the severe phenotypes (32). We decided to further characterize this allele to find out the linkage between T-DNA insertion in *EXO70A1* and ES2 resistance. We analyzed the homozygous mutant at the transcription level and found that it accumulated the 5' end of the *EXO70A1* mRNA upstream of the T-DNA insertion site whereas the 3' end of mRNA downstream of the T-DNA insertion was not detected (Fig. 3 F and G). We suspected that this mutation resulted in dominant resistance due to the truncated mRNA encoding a stably accumulated N-terminal peptide that caused the severe phenotypic defect in *exo70A1-3*. In contrast, *exo70A1-1* and *-2* were reported as null and knockdown alleles that exhibit a milder phenotype (7). This observation led us to characterize the mutant allele at the protein level.

The expected mass of the truncated peptide was  $\sim$ 25 kDa, with 231 amino acids. Because the anti-EXO70A1 antibodies did not recognize the N-terminal region of EXO70A1, we took advantage of mass spectrometry analysis. We first surveyed the *E. coli*-

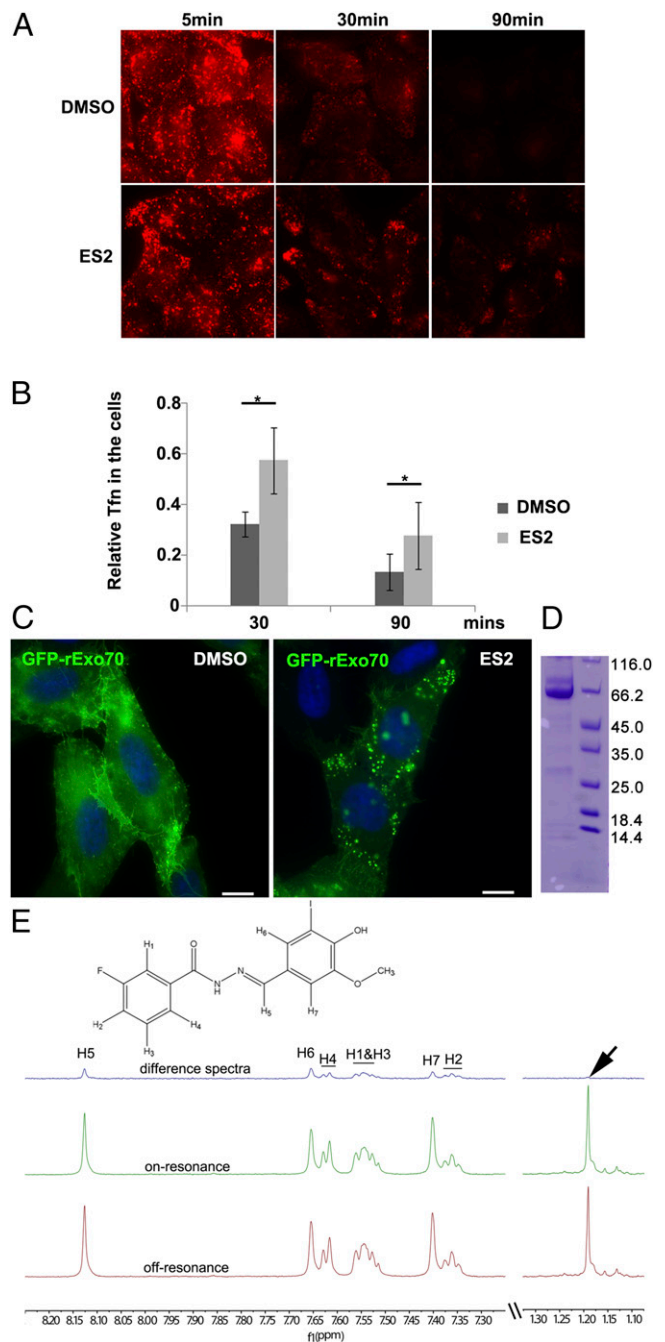


**Fig. 5.** ES2 targets EXO70 to inhibit exocytosis in mammalian cells. (A) ES2 treatment inhibits the recycling of transferrin in HeLa cells. Time course images of HeLa cells transfected with Alexa488-transferrin that were chased in the presence of DMSO (Top) or ES2 (Bottom). (B) The amount of transferrin retained in cells after 30 min and 90 min of chasing at 37  $^{\circ}$ C relative to that after 5 min chasing in corresponding DMSO- or ES2-treated cells. The error bars represent SD from three independent experiments. One hundred cells were analyzed per experiment.  $*P < 0.05$  by paired two-sample t test. (C) ES2 inhibits plasma membrane localization of GFP-rEXO70 in HeLa cells. Upon ES2 treatment, GFP-rEXO70 is accumulated in intracellular compartments (Right). (D) Coomassie blue staining of purified rat EXO70 protein (left lane) used for STD-NMR experiment. (E) The spectra of the STD-NMR experiment show interaction between ES2 and rEXO70A1. The off-resonance spectrum, the on-resonance spectrum, and the different spectrum are shown in red, green, and blue, respectively. The arrow indicates a spectral peak from the buffer component that does not show in the different spectrum. (Scale bars: 10  $\mu$ m.)

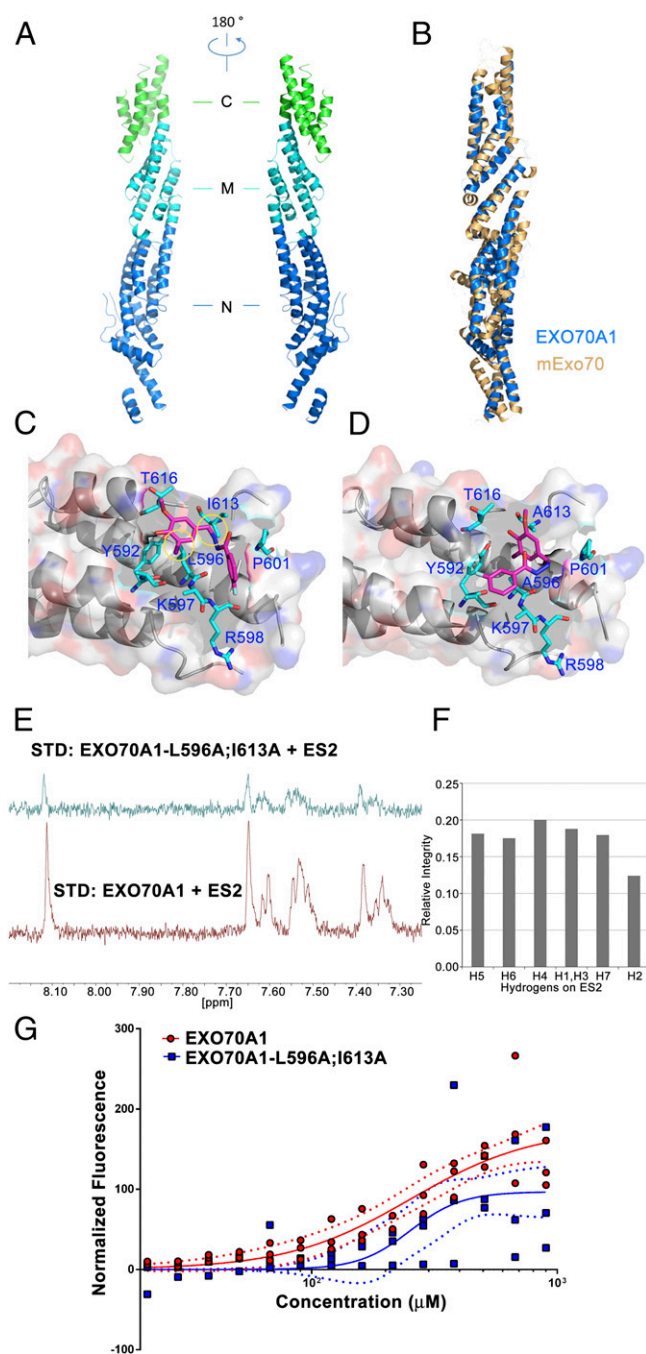


**Fig. 6.** EXO70A1 amino acids L596 and I613 participate in interaction with ES2. (A) Structure of EXO70A1. The structure is divided into three domains: N-terminal domain (blue), C-terminal domain (green), and middle domain (cyan). (B) Structural superposition of EXO70A1 with mEXO70. (C) Conformation of the EXO70A1-ES2 complex from docking simulation. ES2 (magenta) fits in the cavity that is formed by several amino acids (cyan). The two yellow circles highlight the two amino acids L596 and I613 that were mutated to A as shown in D. (D) Conformation of the EXO70A1-L596A;I613A-ES2 complex from docking simulation. With the two mutations at L596 and I613, ES2 conformation is changed in comparison with the WT EXO70A1 protein. (E) STD-NMR profiles of EXO70A1 (Bottom) and EXO70A1-L596A;I613A (Top) with ES2 when using the same concentrations of protein and ES2. The spectra are presented in the same scale. The integrity of an individual STD-NMR spectrum is less in reactions with mutant protein in comparison with the reactions using a WT protein. (F) The ratio of STD-NMR spectral integrity of different protons in ES2 between EXO70A1-L596A;I613A and EXO70A1 shown in E. In the EXO70A1-L596A;I613A mutant protein, the integrities of the STD-NMR spectral peaks in ES2 are reduced to about 20% of the WT EXO70A1 protein. (G) Thermophoresis

expressed EXO70A1 protein with nano-LC/MS/MS (liquid chromatography/mass spectrometry/mass spectrometry) and identified a peptide ion from its N-terminal region (amino acids 90–109) with strong signal intensity (Fig. S7). Using this peptide ion with known  $m/z$ , charge state, and retention time as the fingerprint for EXO70A1, we then analyzed plant proteins derived from WT and the T-DNA line. We analyzed SDS gel bands with approximate masses of 70 kDa and 25 kDa, respectively, from both the WT and *exo70A1-3* mutant using nano-LC/MS (the system was confirmed with no background after blank injection). It was found that the amino acid 90–109 fingerprint was detected in WT 70-kDa and *exo70A1-3* 25-kDa samples (Fig. 3H), indicating that the *exo70A1-3* allele accumulates a truncated peptide in planta that might be responsible for the ES2 resistance. To test the contribution of the truncated peptide to the growth resistance of the *exo70A1-3* mutant, we expressed EXO70A1 amino acids 1–231 in WT plants under the Cauliflower Mosaic Virus 35S promoter and then analyzed the effect of ES2 on the transgenic lines. Homozygous transgenic lines expressing the N terminus of EXO70A1 showed partial resistance to ES2 in root growth when grown on media containing lower concentrations of ES2 (Fig. 3I). We also found resistance to ES2 when *exo70A1-3* heterozygous seedlings or EXO70A1 N terminus expression seedlings were transferred from normal media to ES2-containing media (Fig. 3J). Reproduction of ES2 resistance in transgenic lines confirmed the linkage between EXO70A1 N terminus expression and ES2 resistance. Similar to *exo70A1-3* heterozygous plants, plants expressing the N-terminal truncated peptide displayed normal growth at the seedling stage in the absence of ES2, but retarded growth, small stature, reduced seed yield, and flower development defects after bolting on soil (Fig. S8). Thus, we concluded that the EXO70A1 N-terminal peptide was sufficient to induce dominant ES2 resistance in plants, and this observation confirmed in planta that EXO70A1 was a target of ES2. This observation also suggested that the exocyst could be an important site for controlling the dynamics between recycling to the plasma membrane and vacuole targeting and that the N-terminal domain probably served distinct roles in exocyst regulation. Heterozygous *exo70A1-3* plants show developmental phenotypes in later stages of plant development, which is similar to the EXO70A1 N-terminal peptide expression line. This observation may also reflect the regulatory roles of the EXO70A1 N-terminal domain and the contribution of EXO70A1 to different stages of plant development. Although further investigation is needed to understand the underlying cellular mechanisms for the roles of the EXO70A1 N terminus region in regulating exocytosis and in plant development, the genetic resistance in the mutant and transgenic lines confirms the linkage between ES2 and exocyst regulation at the genetic level.

**ES2 Inhibits Cellular Dynamics of EXO70A1.** To discover whether ES2 inhibited EXO70 cellular dynamics directly, we examined the cellular localization of GFP-tagged EXO70A1 (GFP:EXO70A1) in *Arabidopsis* root cells upon ES2 treatment. GFP:EXO70A1 showed plasma membrane localization with distinct polarized maximum at the outer lateral side of root epidermal cells in the root tip (Fig. 4A, white arrows). We found that, upon ES2 treatment, the polarized localization pattern of EXO70A1 was lost (Fig. 4A–C). Plot of fluorescence intensity across the root transition zone in DMSO-treated control seedlings revealed high

binding curves of NT-647-labeled purified EXO70A1 and EXO70A1-L596A;I613A titrated with different concentrations of ES2. Red circles and blue squares represent the normalized fluorescence of EXO70A1 and EXO70A1-L596A;I613A, respectively, in each triplicate experiment. Solid lines represent the nonlinear fit curves, and the dotted lines around the fit curve represent the 95% confidence interval of the fit.



**Table 3. Data collection and refinement statistics**

Data collection and statistics	EXO70A1(Se-MET)
Data collection	
Space group	$P2_12_1$
Cell dimensions	
<i>a</i> , <i>b</i> , <i>c</i> , Å	55.1, 72.1, 327.9
<i>a</i> , <i>b</i> , <i>g</i> , °	90, 90, 90
Wavelength	0.9774
Resolution, Å	50.0–3.40 (3.52–3.40)*
$R_{\text{sym}}$ or $R_{\text{merge}}$	0.097(0.404)
$I/\sigma I$	19.7(3.3)
Completeness, %	99.9(99.7)
Redundancy	4.6(4.3)
Refinement	
Resolution, Å	48.5–3.40
No. of reflections	34,418
$R_{\text{work}}/R_{\text{free}}$	0.312/0.337
No. of atoms	
Protein	5,886
<i>B</i> -factors	
Protein	116.1
rmsd	
Bond lengths, Å	0.010
Bond angles, °	1.497
Ramachandran plot	
Favored regions, %	94.0
Allowed regions, %	5.8
Outliers, %	0.2

\*Values in parentheses are for the highest resolution shell.

fluorescence intensity in the outside layer of the root epidermal cells (Fig. 4B). After 2 h of 40  $\mu$ M ES2 treatment, the lateral polarity of EXO70A1 was changed, as reflected by reduced fluorescence intensity at the outside layer of root epidermal cells (Fig. 4C). The mean fluorescence intensity of lateral GFP:EXO70A1 in ES2-treated seedlings ( $32.0 \pm 12.2$ , mean  $\pm$  SD,  $n = 10$ ) was significantly lower than DMSO control seedlings ( $88.1 \pm 18.6$ , mean  $\pm$  SD,  $n = 10$ ) ( $P < 0.05$ ). However, the lateral polarity pattern of two other exocyst components, EXO84 and SEC8, was not affected (Fig. S9A, white arrows). In root hair cells, where active exocytosis is required for polarized growth (33, 34), it was found that, upon ES2 treatment, the fluorescence recovery of GFP:EXO70A1 after photobleaching was significantly slower compared with control cells (Fig. 4D). The maximum fluorescence recovery was more than 80% of the prebleached intensity within 3 min in control cells whereas the fluorescence recovery was limited to 20% of the prebleached level at the same time in cells treated with ES2 (Fig. 4E). This result indicated that ES2 significantly inhibited the cellular dynamics of EXO70A1 in root hair cells as well. The fact that ES2 strongly interfered with EXO70A1 localization without perturbing two other exocyst subunits further supported that, in planta, EXO70A1 was a target of ES2. The specificity of mislocalization suggests that the mechanism of EXO70A1 lateral plasma membrane targeting is distinct from that of other exocyst components. Furthermore, EXO70A1 may dissociate from the complex independently from other subunits, indicating that the maintenance of its lateral polarity may be distinct (assuming that EXO84, SEC8, and EXO70A1 are part of the exocyst while at the lateral plasma membrane). Furthermore only lateral polarity was affected (not isolar lateral localization), indicating that EXO70A1 lateral polarity is distinct.

**ES2 Targets EXO70 to Inhibit Recycling in Mammalian Cells.** Due to the evolutionary conservation of the composition and function of the exocyst complex, we were interested in investigating whether

ES2 can target EXO70 in other systems. We examined whether ES2 would affect exocytosis in human cells using the transferrin (Tfn) recycling assay, which measures the recycling of endocytosed transferrin to the plasma membrane. The assay has been commonly used to study protein trafficking to the plasma membrane. After treatment with DMSO as a control or ES2 for 1 h, the cells were pulsed with Tfn-AlexaFluor488 on ice for 5 min and chased with complete media to track Tfn trafficking over time. Most of the Tfn was exocytosed after a 90-min chase in cells treated with DMSO (Fig. 5A). However, Tfn accumulated markedly at the protrusion sites of cells treated with ES2, indicating that exocytosis was reduced. Comparison of the ratio of Tfn retention at 30 min and 90 min after chasing with that of 5 min after chasing in DMSO- and ES2-treated cells indicated reduced Tfn trafficking in ES2-treated cells (Fig. 5B). To test whether the reduced exocytosis in mammalian cells was related to EXO70 as in plants, we tested the localization of GFP-tagged rat EXO70 (rEXO70) protein after ES2 treatment. We found that ES2 treatment induced the accumulation of EXO70 vesicles near the plasma membrane (Fig. 5C). A similar effect was observed for human EXO70 isoform2 and isoform5 proteins upon ES2 treatment (Fig. S9B). These vesicles may suggest a block of vesicle tethering and fusion with plasma membrane. To test direct interaction between ES2 and rEXO70, we purified *E. coli*-expressed rEXO70 (Fig. 5D) and performed an STD-NMR experiment. The interaction between ES2 and rEXO70 was confirmed by the presence of saturation energy transfer (Fig. 5E). These data confirm that ES2 directly targets EXO70 in vivo to inhibit exocytosis in mammalian cells as well as in plants. It further indicates that, in human cells, ES2 can target multiple isoforms of EXO70, resulting in misregulation of exocytosis.

The fact that plant and mammalian EXO70 proteins are targets of ES2 suggests structural similarity. To better understand the structural basis for the conservation of the altered regulation of EXO70A1 by ES2, we crystallized *Arabidopsis* EXO70A1 and determined its structure at 3.1-Å resolution. The crystal structure of EXO70A1 revealed that it adopted an elongated architecture resembling that previously observed for yeast (35, 36) and mouse EXO70 (mEXO70) (37). We were able to trace 17  $\alpha$ -helices in the structure, which were further divided into three domains based on interdomain hinge points and the overall arrangement of helices: N-terminal (75–379), C-terminal (511–629), and middle (380–510) connecting the N- and C-terminal domains (Fig. 6A) (36). The relative conformations of the three domains in EXO70A1 and mEXO70 were similar, except for a slight difference in the orientation of the N-terminal domain. Superposition of the middle C-terminal domains of EXO70A1 and mEXO70 gave a root mean square deviation (rmsd) of 1.59 Å on 147 C $\alpha$  atoms (Fig. 6B). We were able to trace all of the helices in the final structure, except that a number of loops connecting the helices were missing due to poor electron density. The statistics for the X-ray diffraction data and structure are summarized in Table 3. Such a high structural similarity suggested that, despite low sequence identity (32% in middle C-terminal domains), the biochemical functions of plant and mammalian EXO70 proteins were most likely conserved. This result supported our conclusion that ES2 targets EXO70 in plants and three mammals (rats, humans, and, probably, mice).

With an available crystal structure of EXO70A1, a molecular docking tool, Autodock, was applied to predict possible ES2 binding sites of the EXO70A1, by fixing the protein and allowing ES2 to freely bind to several potential pockets of the EXO70A1. We decided to use molecular docking to predict possible ES2 binding sites on EXO70A1. Using Autodock (38), we found one possible binding pocket located at the C terminus of EXO70A1. The binding cavity was principally composed of the hydrophobic amino acids Y592, L596, K597, P601, R598, I613, and T616 (Fig. 6C). The conformation of ES2 can fit well in the C-terminal

pocket of the WT EXO70A1 protein. The fluorine-containing aromatic ring of ES2 locates in the cavity created by P601, R598, and K597 main chains. The iodine-containing aromatic ring is surrounded by hydrophobic sidechains of several residues, including I613, L596, Y592, and T616. When we performed the docking with mutations of L596 and I613 to Ala, the binding pocket became larger because of the missing of I613 and L596 sidechains. However, in this case, the ES2 conformation couldn't fit the pocket properly (Fig. 6D). Although the iodine-containing aromatic ring remained deeply in the pocket and formed interactions with A613, fewer interactions between the fluoride-containing aromatic ring and Y592/A596 were shown. In addition, in contrast to WT EXO70A1, the L596A and I613A mutations resulted in missing attractions between the ES2 and P601, R598, and T616, which would generate higher binding free energy and a weaker ligand-binding mode. To confirm that the predicted pocket plays a role in ES2 binding, we mutated amino acids L596 and I613 to Alanine (L596A;I613A) and tested for the binding activity of mutant protein to ES2 using STD-NMR. We found that, under the same protein and ES2 concentrations, L596A;I613A had less binding to ES2, which was reflected by reduced STD-NMR integral integrity (Fig. 6E and F and Fig. S10A and B). This observation was consistent with the prediction that L596 and I613 participate in interaction with ES2 although the mutations did not completely abolish the interaction between EXO70A1 and ES2. We also compared the thermophoretic mobility of EXO70A1 and EXO70A1-L596A;I613A when titrated with ES2 (Fig. 6G). Although the maximal thermophoretic mobility was lower for the mutated protein than for EXO70A1, the  $K_d$  of  $252 \pm 50.6$  for the interaction of ES2 with EXO70A1-L596A;I613A is not significantly different at a 95% level of confidence than the  $K_d$  for ES2 with EXO70A1 (Table 2). Despite this result, the nonlinear fit for the interaction of ES2 with EXO70A1 is more robust with an R-squared of 81.7% than for the interaction of ES2 with EXO70A1-L596A;I613A, with an R-squared of 46.5%. This observation suggested that amino acids L596 and I613 were not essential for binding of ES2 but may interact with binding site residues and indirectly affect the local binding microenvironment. Amino acids L596 and I613 are conserved between *Arabidopsis* EXO70A1 and mammalian EXO70 proteins (Fig. S10C), explaining why ES2 could interact with both *Arabidopsis* EXO70A1 and rat EXO70.

## Discussion

In summary, the previously unidentified small molecule ES2 directly interacts with and inhibits the dynamics of the evolutionarily conserved EXO70 proteins to reduce exocytosis in plants and mammals and enhance plant vacuolar trafficking. Expression of the EXO70A1 N terminus in WT plants partially overcomes the effects of ES2, indicating that this region might positively regulate plasma membrane docking of the full-length protein. Despite the high divergence in their primary protein structure, plant and mammalian EXO70 proteins share an evolutionarily conserved structure that likely permits ES2 to target EXO70 proteins in plants and humans. This result is the first re-

port, to our knowledge, of the structure of a plant EXO70 subunit. The similarities in 3D structure strongly support a conservation of exocyst function and functional sites during evolution. Despite these new details, it is unclear how the exocyst is integrated within the context of the endomembrane trafficking system in multicellular organisms. In *Arabidopsis*, there are 23 genes encoding EXO70 isoforms, more than in mammals or yeast. Most of these isoforms are poorly defined in terms of function. Our result in human cells is powerful in that it indicates that ES2 will probably target many EXO70 isoforms and shows the power of chemical genomics in addressing genetic redundancy. It also indicates that, by using a high content, cell biology-based pollen screen for modulators of endomembrane trafficking, we have found a molecule that will permit us to investigate the basic functional domains of EXO70. Although beyond the scope of this study, the functional roles of the N-terminal and C-terminal domains now can be investigated in more detail to understand the regulation of exocyst-related vesicle transport processes, especially the dynamics and regulation of trafficking toward the vacuole or plasma membrane, which are altered by ES2. The structure of EXO70A1 will also be of value in further modeling the ES2 binding site.

This approach may also provide a new avenue toward novel drugs. To date, we are not aware of any small molecules that target the exocyst; thus, this discovery presents a novel drug target. It also allows further development of similar drugs with higher affinity to EXO70, with stronger drug activity in controlling exocytosis. The exact role of the exocyst in human diseases requires further investigation. It may be possible to increase the potency and modify the isoform specificity of ES2 or similar molecules targeting EXO70 to control EXO70-related human diseases, such as cancer cell invasions and diabetes, which involves glucose transport. Although the sequence identity between plant EXO70s and yeast EXO70 is lower than that of mammalian cells, we found that I613 is conserved between plant and yeast EXO70s. It is possible that ES2 can target yeast EXO70 as well and thus can be a potential tool in fungal pathogen manipulation.

## Materials and Methods

DARTS and STD-NMR assays were developed from published protocols (39, 40). The EXO70A1 protein was expressed in *E. coli* and purified for STD-NMR, MST, and crystallization experiments. The sources of *Arabidopsis* transgenic lines and the detailed methods are listed in *SI Materials and Methods*.

**Dataset S1** contains information on  $^1\text{H}$ ,  $^{13}\text{C}$ , and  $^{19}\text{F}$  NMR spectra of the synthesized compounds, and **Dataset S2** contains information on the peptides detected from the pull-down assay using biotin-tagged analogs combined with mass spectrometry analysis.

**ACKNOWLEDGMENTS.** We thank Jocelyn Brimo (University of California, Riverside) for administrative support. We thank Dr. Jiri Friml for comments on the manuscript. We thank Dr. David Carter for assistance with microscopy. US Department of Energy Grant DE-FG02-02ER15295 provided financial support (to N.V.R. and G.R.H.). The National Aeronautics and Space Administration provided financial support with Grant NNX09AK82G (to G.K.M.). Grantová Agentura České Republiky/Czech Science Foundation Project 15-148865 and Ministerstvo Školství, Mládeže a Tělovýchovy České Republiky Project NPUI LO1417 provided support (to V.Z.).

- Novick P, Field C, Schekman R (1980) Identification of 23 complementation groups required for post-translational events in the yeast secretory pathway. *Cell* 21(1):205–215.
- Zhao Y, et al. (2013) Exo70 generates membrane curvature for morphogenesis and cell migration. *Dev Cell* 26(3):266–278.
- Fujita A, et al. (2013) GTP hydrolysis of TC10 promotes neurite outgrowth through exocytic fusion of Rab11- and L1-containing vesicles by releasing exocyst component Exo70. *PLoS One* 8(11):e79689.
- Dupraz S, et al. (2009) The TC10-Exo70 complex is essential for membrane expansion and axonal specification in developing neurons. *J Neurosci* 29(42):13292–13301.
- Zuo X, et al. (2006) Exo70 interacts with the Arp2/3 complex and regulates cell migration. *Nat Cell Biol* 8(12):1383–1388.
- Xiong X, et al. (2012) An association between type IV PI4P 5-kinase and Exo70 directs E-cadherin clustering and epithelial polarization. *Mol Biol Cell* 23(1):87–98.
- Synek L, et al. (2006) AtEXO70A1, a member of a family of putative exocyst subunits specifically expanded in land plants, is important for polar growth and plant development. *Plant J* 48(1):54–72.
- Kulich I, et al. (2010) Arabidopsis exocyst subunits SEC8 and EXO70A1 and exocyst interactor ROH1 are involved in the localized deposition of seed coat pectin. *New Phytol* 188(2):615–625.
- Fendrych M, et al. (2010) The Arabidopsis exocyst complex is involved in cytokinesis and cell plate maturation. *Plant Cell* 22(9):3053–3065.
- Pečenková T, et al. (2011) The role of the exocyst complex subunits Exo70B2 and Exo70H1 in the plant-pathogen interaction. *J Exp Bot* 62(6):2107–2116.
- Kulich I, et al. (2013) Arabidopsis exocyst subcomplex containing subunit EXO70B1 is involved in autophagy-related transport to the vacuole. *Traffic* 14(11):1155–1165.
- Zárský V, Kulich I, Fendrych M, Pečenková T (2013) Exocyst complexes multiple functions in plant cells secretory pathways. *Curr Opin Plant Biol* 16(6):726–733.

13. Inoue M, Chang L, Hwang J, Chiang SH, Saltiel AR (2003) The exocyst complex is required for targeting of Glut4 to the plasma membrane by insulin. *Nature* 422(6932):629–633.
14. Lu H, et al. (2013) Exo70 isoform switching upon epithelial-mesenchymal transition mediates cancer cell invasion. *Dev Cell* 27(5):560–573.
15. Liu J, Yue P, Artym VV, Mueller SC, Guo W (2009) The role of the exocyst in matrix metalloproteinase secretion and actin dynamics during tumor cell invadopodia formation. *Mol Biol Cell* 20(16):3763–3771.
16. Drakakaki G, et al. (2011) Clusters of bioactive compounds target dynamic endomembrane networks in vivo. *Proc Natl Acad Sci USA* 108(43):17850–17855.
17. Robert S, et al. (2008) Endosidin1 defines a compartment involved in endocytosis of the brassinosteroid receptor BR1 and the auxin transporters PIN2 and AUX1. *Proc Natl Acad Sci USA* 105(24):8464–8469.
18. Geldner N, et al. (2003) The Arabidopsis GNOM ARF-GEF mediates endosomal recycling, auxin transport, and auxin-dependent plant growth. *Cell* 112(2):219–230.
19. Jaillais Y, Fobis-Loisy I, Miège C, Rollin C, Gaude T (2006) AtSNX1 defines an endosome for auxin-carrier trafficking in Arabidopsis. *Nature* 443(7107):106–109.
20. Kleine-Vehn J, et al. (2008) Differential degradation of PIN2 auxin efflux carrier by retromer-dependent vacuolar targeting. *Proc Natl Acad Sci USA* 105(46):17812–17817.
21. Robert S, et al. (2010) ABP1 mediates auxin inhibition of clathrin-dependent endocytosis in Arabidopsis. *Cell* 143(1):111–121.
22. Tamura K, et al. (2003) Why green fluorescent fusion proteins have not been observed in the vacuoles of higher plants. *Plant J* 35(4):545–555.
23. Drdová EJ, et al. (2013) The exocyst complex contributes to PIN auxin efflux carrier recycling and polar auxin transport in Arabidopsis. *Plant J* 73(5):709–719.
24. Chong YT, et al. (2010) Characterization of the Arabidopsis thaliana exocyst complex gene families by phylogenetic, expression profiling, and subcellular localization studies. *New Phytol* 185(2):401–419.
25. Li S, et al. (2010) Expression and functional analyses of EXO70 genes in Arabidopsis implicate their roles in regulating cell type-specific exocytosis. *Plant Physiol* 154(4):1819–1830.
26. Hála M, et al. (2008) An exocyst complex functions in plant cell growth in Arabidopsis and tobacco. *Plant Cell* 20(5):1330–1345.
27. Lomenick B, et al. (2009) Target identification using drug affinity responsive target stability (DARTS). *Proc Natl Acad Sci USA* 106(51):21984–21989.
28. Lepre CA, Moore JM, Peng JW (2004) Theory and applications of NMR-based screening in pharmaceutical research. *Chem Rev* 104(8):3641–3676.
29. Dühr S, Braun D (2006) Why molecules move along a temperature gradient. *Proc Natl Acad Sci USA* 103(52):19678–19682.
30. Seidel SA, et al. (2013) Microscale thermophoresis quantifies biomolecular interactions under previously challenging conditions. *Methods* 59(3):301–315.
31. Wienken CJ, Baaske P, Rothbauer U, Braun D, Dühr S (2010) Protein-binding assays in biological liquids using microscale thermophoresis. *Nat Commun* 1:100.
32. Rybak K, et al. (2014) Plant cytokinesis is orchestrated by the sequential action of the TRAPP1 and exocyst tethering complexes. *Dev Cell* 29(5):607–620.
33. Wen TJ, Hochholdinger F, Sauer M, Bruce W, Schnable PS (2005) The roothairless1 gene of maize encodes a homolog of sec3, which is involved in polar exocytosis. *Plant Physiol* 138(3):1637–1643.
34. Zárský V, Cvrcková F, Potocký M, Hála M (2009) Exocytosis and cell polarity in plants - exocyst and recycling domains. *New Phytol* 183(2):255–272.
35. Dong G, Hutagalung AH, Fu C, Novick P, Reinisch KM (2005) The structures of exocyst subunit Exo70p and the Exo84p C-terminal domains reveal a common motif. *Nat Struct Mol Biol* 12(12):1094–1100.
36. Hamburger ZA, Hamburger AE, West AP, Jr, Weis WI (2006) Crystal structure of the *S.cerevisiae* exocyst component Exo70p. *J Mol Biol* 356(1):9–21.
37. Moore BA, Robinson HH, Xu Z (2007) The crystal structure of mouse Exo70 reveals unique features of the mammalian exocyst. *J Mol Biol* 371(2):410–421.
38. Morris GM, et al. (1998) Automated docking using a Lamarckian genetic algorithm and an empirical binding free energy function. *J Comput Chem* 19(14):1639–1662.
39. Lomenick B, Jung G, Wohlschlegel JA, Huang J (2011) Target identification using drug affinity responsive target stability (DARTS). *Curr Protoc Chem Biol* 3(4):163–180.
40. Viegas A, Manso J, Nobrega FL, Cabrita EJ (2011) Saturation-transfer difference (STD) NMR: A simple and fast method for ligand screening and characterization of protein binding. *J Chem Educ* 88(7):990–994.
41. Fendrych M, et al. (2013) Visualization of the exocyst complex dynamics at the plasma membrane of Arabidopsis thaliana. *Mol Biol Cell* 24(4):510–520.
42. Geldner N, et al. (2009) Rapid, combinatorial analysis of membrane compartments in intact plants with a multicolor marker set. *Plant J* 59(1):169–178.
43. Ueda T, Uemura T, Sato MH, Nakano A (2004) Functional differentiation of endosomes in Arabidopsis cells. *Plant J* 40(5):783–789.
44. Xu J, Scheres B (2005) Dissection of Arabidopsis ADP-RIBOSYLATION FACTOR 1 function in epidermal cell polarity. *Plant Cell* 17(2):525–536.
45. Wisniewska J, et al. (2006) Polar PIN localization directs auxin flow in plants. *Science* 312(5775):883.
46. Fu Y, Xu T, Zhu L, Wen M, Yang Z (2009) A ROP GTPase signaling pathway controls cortical microtubule ordering and cell expansion in Arabidopsis. *Curr Biol* 19(21):1827–1832.
47. Russinova E, et al. (2004) Heterodimerization and endocytosis of Arabidopsis brassinosteroid receptors BR1 and AtSERK3 (BAK1). *Plant Cell* 16(12):3216–3229.
48. Matushima R, Kondo M, Nishimura M, Hara-Nishimura I (2003) A novel ER-derived compartment, the ER body, selectively accumulates a beta-glucosidase with an ER-retention signal in Arabidopsis. *Plant J* 33(3):493–502.
49. Cho M, Lee SH, Cho HT (2007) P-glycoprotein4 displays auxin efflux transporter-like action in Arabidopsis root hair cells and tobacco cells. *Plant Cell* 19(12):3930–3943.
50. Cutler SR, Ehrhardt DW, Griffiths JS, Somerville CR (2000) Random GFP:cDNA fusions enable visualization of subcellular structures in cells of Arabidopsis at a high frequency. *Proc Natl Acad Sci USA* 97(7):3718–3723.
51. Zhang C, Kotchoni SO, Samuels AL, Szymanski DB (2010) SPIKE1 signals originate from and assemble specialized domains of the endoplasmic reticulum. *Curr Biol* 20(23):2144–2149.
52. Surpin M, et al. (2005) The power of chemical genomics to study the link between endomembrane system components and the gravitropic response. *Proc Natl Acad Sci USA* 102(13):4902–4907.
53. Lewis DR, Miller ND, Splitt BL, Wu G, Spalding EP (2007) Separating the roles of acropetal and basipetal auxin transport on gravitropism with mutations in two Arabidopsis multi-drug resistance-like ABC transporter genes. *Plant Cell* 19(6):1838–1850.
54. Carter C, et al. (2004) The vegetative vacuole proteome of Arabidopsis thaliana reveals predicted and unexpected proteins. *Plant Cell* 16(12):3285–3303.
55. Sohn EJ, et al. (2007) The shoot meristem identity gene TFL1 is involved in flower development and trafficking to the protein storage vacuole. *Proc Natl Acad Sci USA* 104(47):18801–18806.
56. Sorenson R, Bailey-Serres J (2014) Selective mRNA sequestration by OLIGOURIDYLATE-BINDING PROTEIN 1 contributes to translational control during hypoxia in Arabidopsis. *Proc Natl Acad Sci USA* 111(6):2373–2378.
57. Emsley P, Cowtan K (2004) Coot: Model-building tools for molecular graphics. *Acta Crystallogr D Biol Crystallogr* 60(Pt 12 Pt 1):2126–2132.
58. Adams PD, et al. (2002) PHENIX: Building new software for automated crystallographic structure determination. *Acta Crystallogr D Biol Crystallogr* 58(Pt 11):1948–1954.
59. Pedretti A, Villa L, Vistoli G (2004) VEGA: An open platform to develop chemo-bioinformatics applications, using plug-in architecture and script programming. *J Comput Aided Mol Des* 18(3):167–173.
60. Gasteiger J, Marsili M (1980) Iterative partial equalization of orbital electronegativity: A rapid access to atomic charges. *Tetrahedron* 36(22):3219–3228.
61. Morris GM, et al. (2009) AutoDock4 and AutoDockTools4: Automated docking with selective receptor flexibility. *J Comput Chem* 30(16):2785–2791.